Supplementary Information

Effect of Rhamnolipid Biosurfactant on Transport and Retention of Iron Oxide Nanoparticles in Water-Saturated Quartz Sand

Shuchi Liao[1], Anushree Ghosh[2,3], Matthew D. Becker[4], Linda M. Abriola[4], Natalie L. Cápiro[5], John D. Fortner[3] and Kurt D. Pennell[1]*

[1] School of Engineering, Brown University, Providence, Rhode Island, 02912, United States

[2] Department of Energy, Environmental, and Chemical Engineering, Washington University in St. Louis, St. Louis, MO, 63130, United States

[3] Department of Chemical and Environmental Engineering, Yale University, New Haven, CT, 06520, United States

[4] Department of Civil and Environmental Engineering, Tufts University, Medford, Massachusetts, 02155, United States

[5] Department of Civil Engineering, Environmental Engineering Program, Auburn University, Auburn, Alabama, 36849, United States

*Corresponding Author:

Kurt D. Pennell, PhD, PE, BCEE

School of Engineering, Brown University
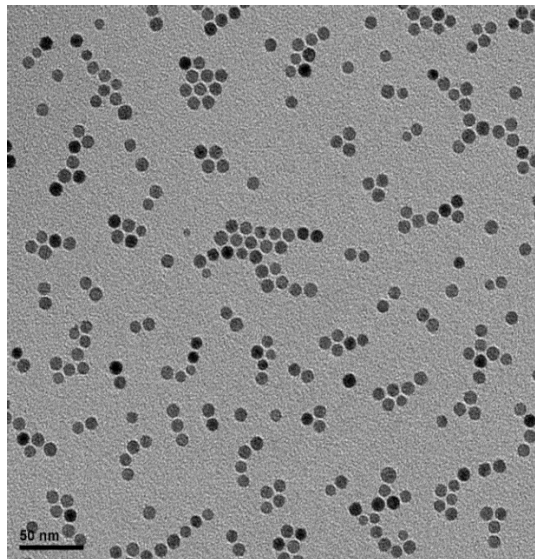
Box D, 184 Hope Street

Providence, RI 02912

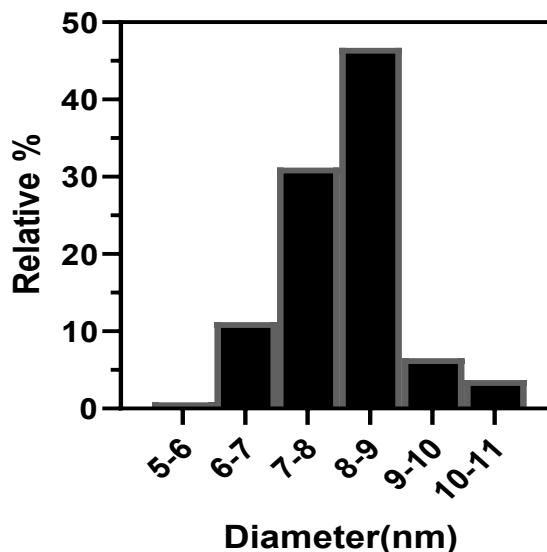office: 401-863-9034

cell: 781-502-8545

Email: kurt_pennell@brown.edu

1. Transmission Electron Microscopy (TEM) Characterization of Oleic Acid Coated Iron Oxide Nanoparticles (IONPs)
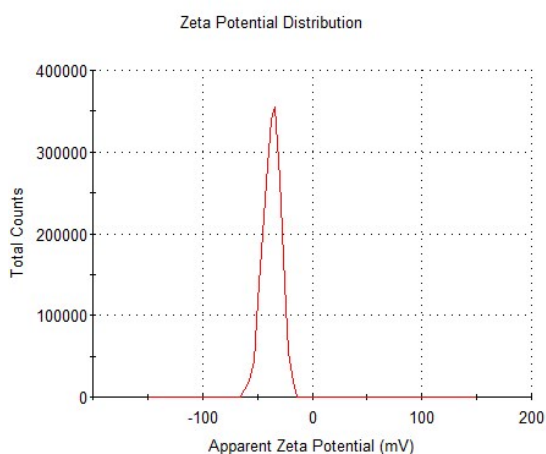
(a)

(b)

(c)

Figure S1. (a) Representative TEM image of oleic-acid coated iron oxide nanoparticles (IONPs). (b) Histogram of diameter range *vs* relative % of frequency of particles analysed using Image J software (U. S. National Institutes of Health, Bethesda, Maryland). TEM samples were prepared by placing a small drop (10 µL) of diluted IONP suspension on a carbon coated copper grids and left to dry at room temperature (22 ± 0.5 °C). The mean IOPN size was determined to be 8nm. (c) Zeta potential distribution of IONP in aerobic medium.
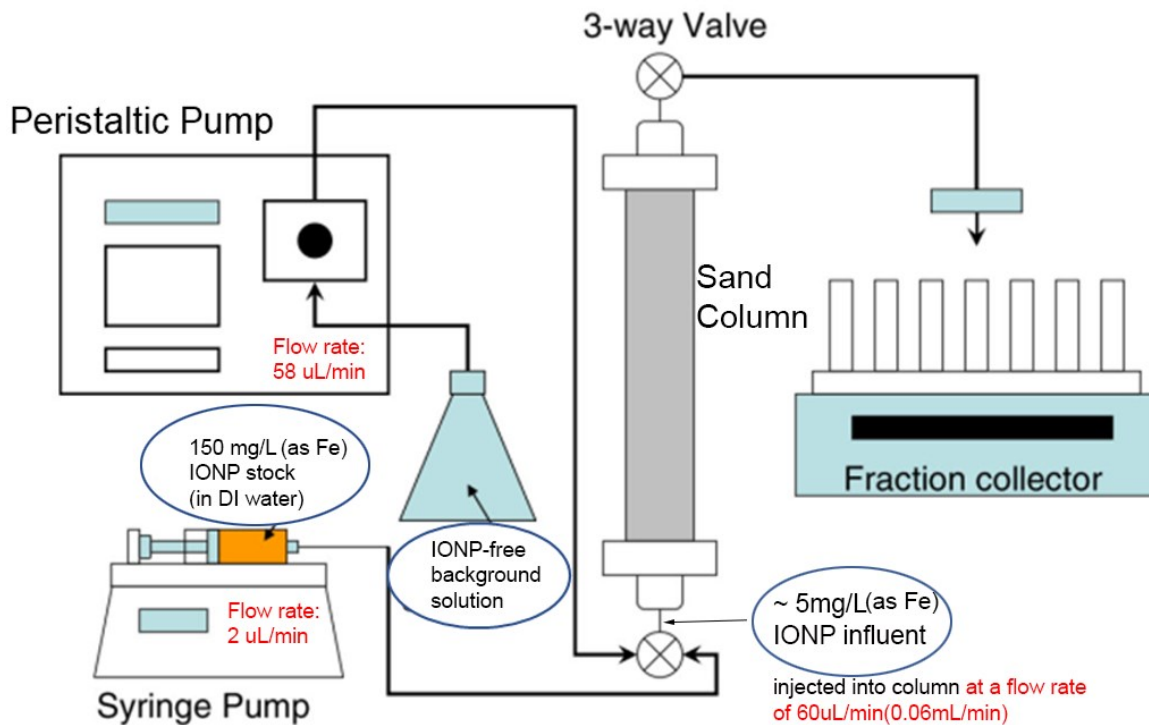
2. Column Experimental Setup

Figure S2. Schematic diagram of one-dimensional column experimental setup. The influent ca.5mg L^{-1} (as iron) IONP solution was prepared by mixing IONP stock solution and the background solution right before the injection to keep a constant influent nanoparticle size/size distribution. For columns incorporating IONP transport with rhamnolipid, rhamnolipid (10 mg L^{-1} or 50mg L^{-1}) was added to background solution beforehand.

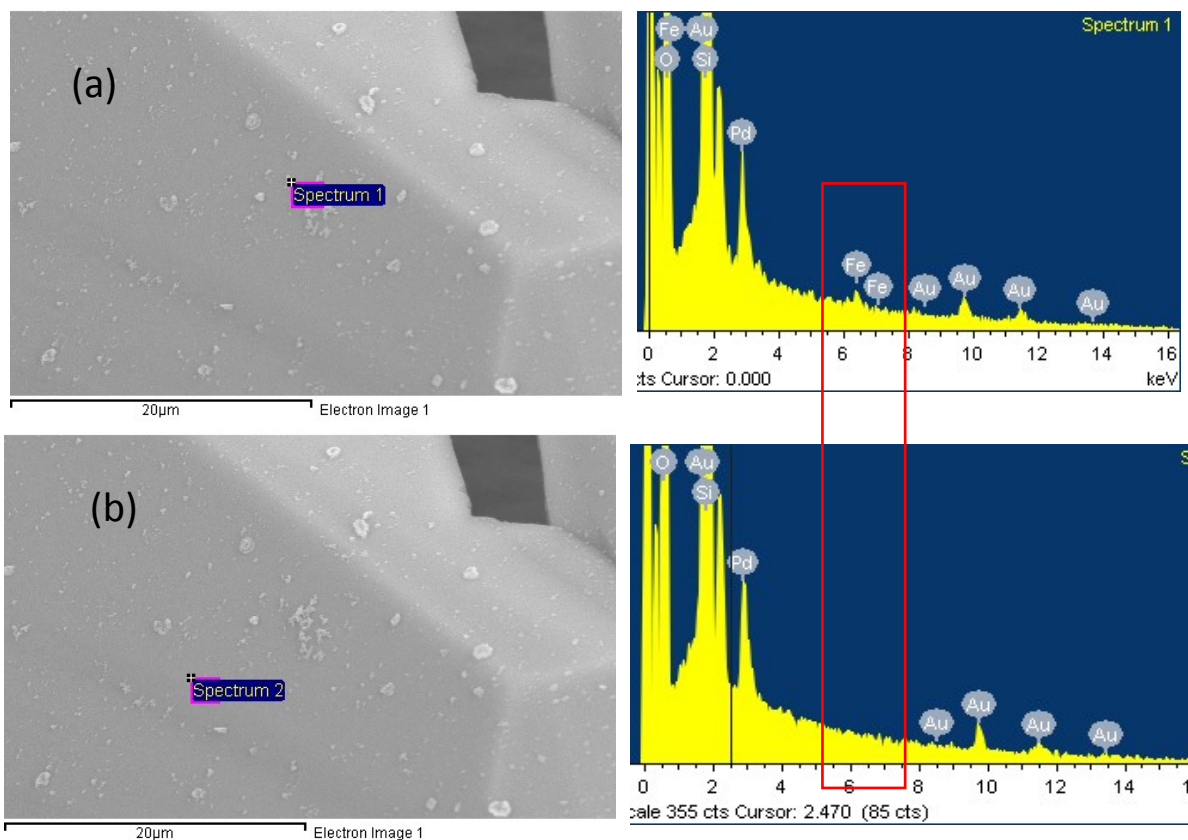**3. Deposition of IONPs Confirmed by Energy Dispersive Spectrometry (EDS)**

Figure S3. EDS imaging of (a) IONPs deposited and (b) bare sand surface. Samples were secured on carbon conductive tape and coated with a layer of gold and platinum prior to EDS analysis (Zeiss LEO 1530 VP SEM). The detected iron amount is 0.45% by weight in spectrum 1, compared to 0% iron in bare sand surface (spectrum 2).

4. Influent Nanoparticle Size Distributions
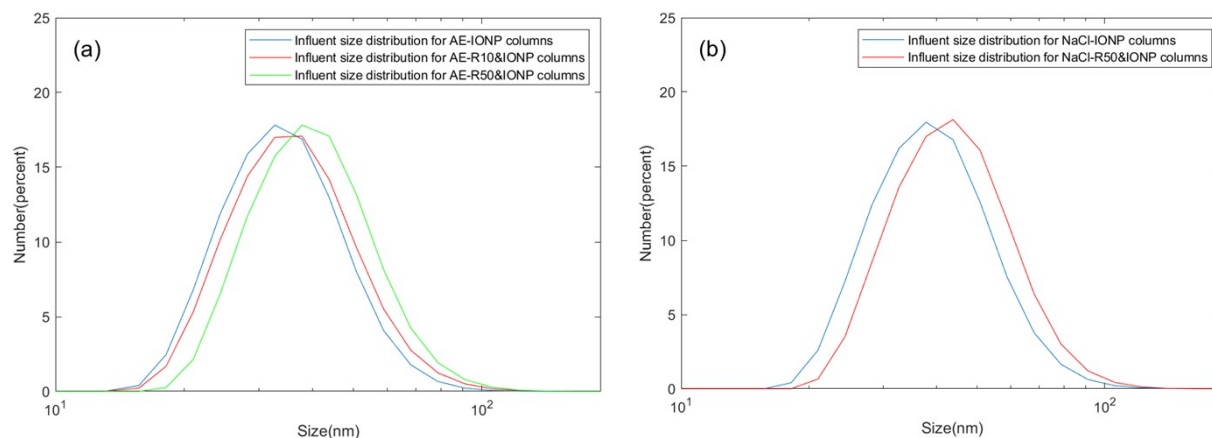
Figure S4. Typical number based influent size distributions for (a) aerobic medium columns when IONP are transported alone(AE-IONP) or with 10 or 50 mg L^{-1} rhamnolipid (AE-R10&IONP or AE-R50&IONP) and (b) 10mM NaCl columns with IONP transported alone (NaCl-IONP) or with 50mg L^{-1} rhamnolipid(NaCl-R50&IONP). The polydispersity indexes (PDIs) for all column influents were lower than 0.2, indicating a monodisperse suspension of injected IONP. The addition of rhamnolipid in the influent slightly increased the IONP size, consistent with the zeta potential results shown in Figure 3b that suggested rhamnolipid was absorbed on IONP surfaces.

5. DLVO Calculations

5.1 Nanoparticle-Nanoparticle Interactions

Derjaguin, Landau, Verwey and Overbeek (DLVO) theory[1, 2] was invoked to evaluate the interactions between nanoparticles in aerobic medium and 10mM NaCl solution. Based on DLVO theory, equations for calculations of Van der Waals interaction and electrostatic interactions are: [3, 4]

$$V_{VDW} = -\frac{A_H}{6k_BT}[\frac{r^2}{h^2+4rh} + \frac{r^2}{h^2+4rh+4r^2} + ln(\frac{r^2+4rh}{h^2+4rh+4r^2})] \qquad (S1)$$

$$V_{EDL} = 64\pi\varepsilon_0\varepsilon\frac{r}{2k_BT}(\frac{k_BT}{e})^2(tanh\frac{e\psi}{4k_BT})^2\exp(-\kappa h) \qquad (S2)$$

Here, h is the distance between nanoparticles, ε_0 is the permittivity of free space, ε is the dielectric constant of water, r is the nanoparticle radius, ψ is the ζ-potential of nanoparticles, κ^{-1} is the Debye-Hückel screening length, and A_H is the Hamaker constant for the IONP-water-IONP system, here 4.0E-20 J. [5]

When rhamnolipid is present in the solution and absorbed on nanoparticle surfaces, steric repulsive interactions were also calculated based on equations presented in Fritz et al, [6] including osmotic interaction:

$$V_{OSM} = 0 \qquad 2d < h$$

$$V_{OSM} = \frac{4\pi r}{v_1}\psi^2(0.5-\chi)\left(d-\frac{h}{2}\right)^2 \qquad d \leq h < 2d$$

$$V_{OSM} = \frac{4\pi r}{v_1}\Phi^2(0.5-\chi)d^2\left(\frac{h}{2d}-0.25-ln\frac{h}{d}\right) \quad h<d \qquad (S3)$$

and elastic repulsion:

$$V_{ELAS} = 0 \qquad d \leq h$$

$$V_{ELAS} = (\frac{2\pi r}{M_W}\Phi d^2\rho_P)(\frac{h}{d}ln\left[\frac{h}{d}\left(\frac{3-\frac{h}{d}}{2}\right)^2\right] - 6ln\left(\frac{3-\frac{h}{d}}{2}\right) + 3(1+\frac{h}{d})^2) \quad h<d \quad (S4)$$

Here, χ is the Flory-Huggins solvency parameter, which is assumed to be 0.286 for rhamnolipid, [7] Φ is the volume fraction of absorbed rhamnolipid within the brush layer, d is the thickness of the rhamnolipid brush layer, and v_1 is the volume of a solvent molecule. Φ was calculated based on the equation reported by Phenra et.al.[3] and d was estimated by the size distribution change shown in Figure S4. Both parameters are summarized in Table S1.

Table S1. Parameters used in calculations of steric repulsion interactions.

	absorbed rhamnolipid (mg L^{-1})	Fraction volume of rhamnolipid Φ	thickness of rhamnolipid brush layer d (nm)
10 mg L^{-1} rhamnolipid in aerobic medium	0.5	0.0021	1.11
50 mg L^{-1} rhamnolipid in aerobic medium	4.5	0.0190	2.98
50 mg L^{-1} rhamnolipid in 10mM NaCl	11	0.0495	2.25

The resulting interaction energy profiles are shown in Figure S5.
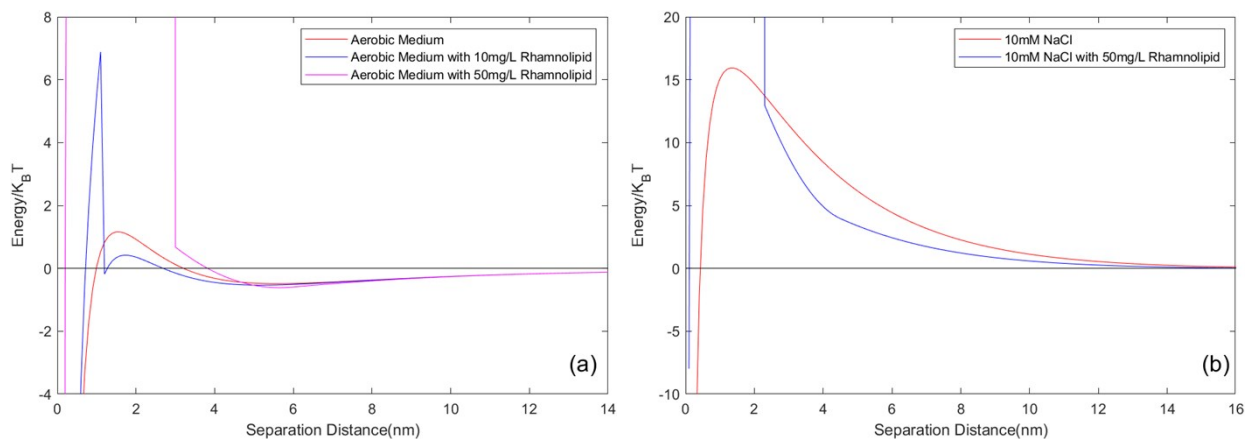

Figure S5. Interaction energy profiles for IONPs in (a) aerobic medium and (b) 10mM NaCl. When rhamnolipid was present in the aerobic medium or 10mM NaCl, steric repulsion was added to the total interactions and resulted a larger energy barrier.

5.2 Nanoparticle-Sand Interactions

DLVO theory can also be applied to the nanoparticle-sand interaction calculation when rhamnolipid is present. In this case, the double layer electrostatic repulsion and Van de Waals attraction between nanoparticle and sand surfaces were calculated as: [8, 9]

$$V_{EDL-ps}$$

$$= \frac{\pi\varepsilon_r\varepsilon_0\kappa(\psi_s^2 + \psi_p^2)}{k_BT} \int_0^a (-coth[\kappa(D + a - a\sqrt{1 - \left(\frac{r}{a}\right)^2})] + coth[\kappa(D + a + a\sqrt{1 - \left(\frac{r}{a}\right)^2}$$

$$[\kappa(D + a - a\sqrt{1 - \left(\frac{r}{a}\right)^2}] - csch[\kappa(D + a + a\sqrt{1 - \left(\frac{r}{a}\right)^2}]\})rdr \ (S5)$$

$$V_{VDW-ps} = -\frac{A_{ps}}{6}\left[\frac{a}{D} + \frac{a}{D + 2a} + \ln\left(\frac{D}{D + 2a}\right)\right] \qquad\qquad (S6)$$

Here, ψ_s and ψ_p are surface potentials of nanoparticles and sand grains, [10] respectively. D is the closest approach from nanoparticle to sand surface. a is the radius of nanoparticles. A_{ps} is the Hamaker constant for IONP-water-quatz(silica) system, here 2.2E-20 J. [11]

The resulting interaction energy profiles of nanoparticle-sand in aerobic medium and 10mM NaCl are shown in Figure S6.
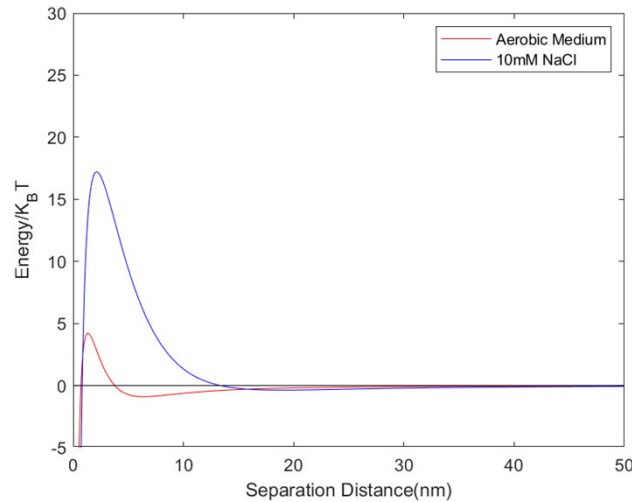

Figure S6. DLVO interaction profiles for IONP and sand grain surface in aerobic medium (IS=50.4mM) and 10mM NaCl solution.

6. Rhamnolipid Only Column Experiments

To obtain rhamnolipid baseline transport data and to estimate retention capacity of Ottawa sands for rhamnolipid, four column experiments were performed using either 10 mg L^{-1} or 50 mg L^{-1} rhamnolipid as the influent. Specifically, ca.5PVs 10 mg L^{-1} in aerobic medium (AE-R10) or 50 mg L^{-1} rhamnolipid in aerobic medium(AE-R50-1 and AE-R50-2) or 50 mg L$^{-1 r}$ in 10mM NaCl solution(NaCl-R50) was injected into water-saturated columns, followed by a 3PV injection of a corresponding rhamnolipid-free background solution. Effluent rhamnolipid concentrations were determined and mass breakthrough was calculated, as summarized in Table S2.

Table S2. Summary of rhamnolipid baseline transport experiments.

Column identifier[a]	Experimental parameters			Mathematically fitted parameters			
	C_0[b]	PW[c]	BT[d]	k_{ads}[e]	Q_{max}[f]	k_{des}[g]	R^2
	(mg L^{-1})	(pv)	(%)	(h^{-1})	(μg g^{-1})	(h^{-1})	
AE-R10	10.3	5.1	82.1	0.03 (0.02,0.04)	3.31 (0.80,5.82)	0.003 (0,0.012)	0.98
AE-R50-1	47.4	4.7	84.7	0.05 (0.04,0.07)	9.41 (6.65,12.17)	0.004 (0,0.011)	0.98
AE-R50-2	52.2	5.0	87.1	0.04 (0.03,0.06)	11.84 (6.73,16.96)	0.004 (0,0.015)	0.97
NaCl-R50	51.7	5.1	77.2	0.20 (0.17,0.23)	13.07 (11.98,14.15)	0.008 (0.003,0.013)	0.99

[a] "AE": Aerobic medium as background electrolyte, "NaCl":10mM NaCl as background electrolyte, "R10": 10 mg L^{-1} rhamnolipid; "R50": 50 mg L^{-1} rhamnolipid; "-1" and "-2" indicate duplicate experiments.

[b] Input rhamnolipid concentration.

[c] Pulse width.

[d] Rhamnolipid breakthrough.

[e] Rhamnolipid adsorption rate coefficient

[f] Maximum retention capacity

[g] Rhamnolipid desorption rate coefficient. The 95% confidence limits of fitted parameters are presented in parentheses. The relatively large 95% confidence intervals for desorption rate indicate that the model predictions are not sensitive to desorption rate under the experimental conditions. Additionally, zero-truncation for the lower bound of CI was used, given that k_{des} are positive values.

The effluent data were fit using a modified filtration model (Figure S7a) with a limiting capacity term and a desorption term, the fitted parameters are listed in Table S2. The rhamnolipid retention profiles were also simulated using the modified filtration model, as shown in Figure S7b.
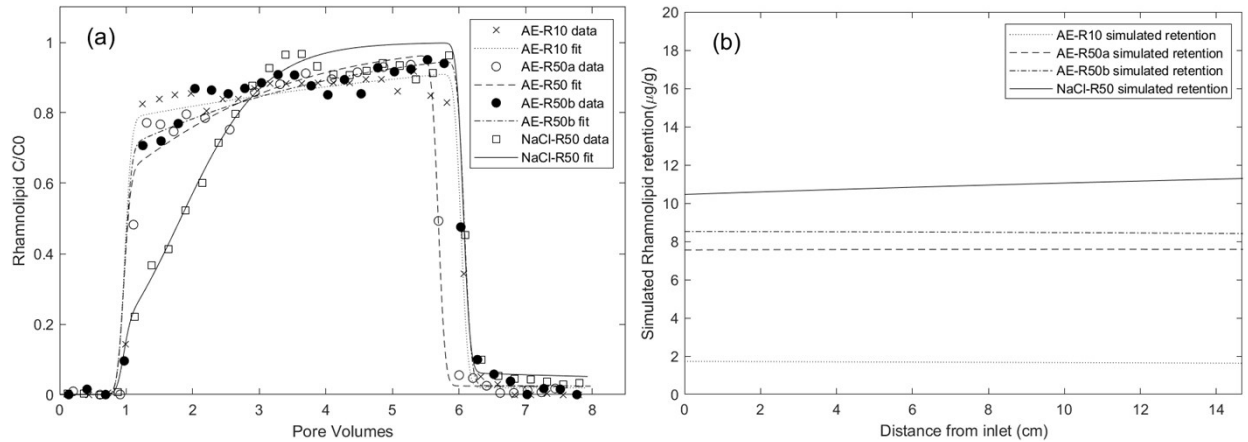

Figure S7. (a) Experimental and fitted effluent BTCs and (b) simulated rhamnolipid retention profiles for 10 mg L^{-1} and 50 mg L^{-1} rhamnolipid transport experiments using aerobic medium as background and 50mg L^{-1} rhamnolipid transport experiments using 10mM NaCl as background in saturated columns packed with 80-100 mesh Ottawa sands at a pore water velocity of 0.43m/day.

Additionally, to verify the retention capacity obtained from rhamnolipid column experiments, batch studies of rhamnolipid sorption on Ottawa sand were also conducted. A Langmuir type isotherm model was used to fit the experimental data in Figure S8.
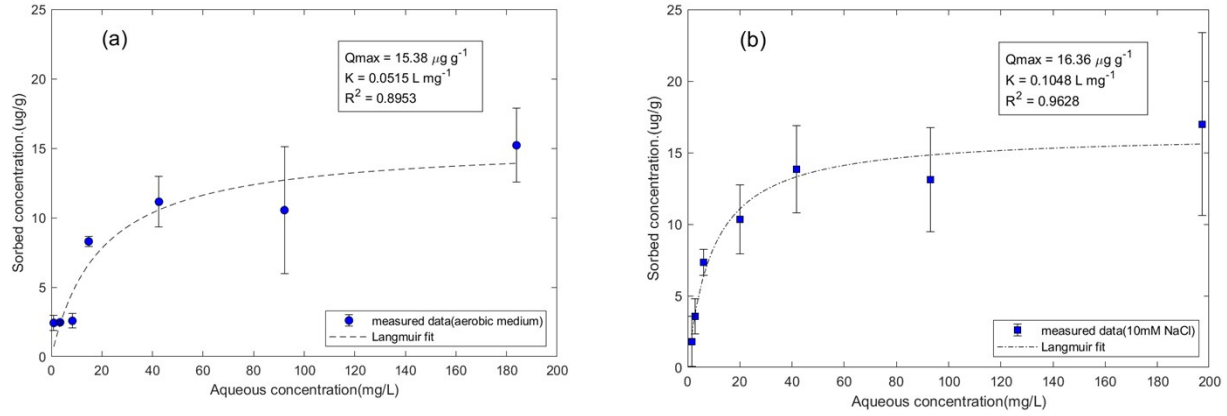
Figure S8. Experimental and Langmuir fitted adsorption isotherm of rhamnolipid on 80-100 mesh Ottawa sand in (a) Aerobic Medium and (b) 10mM NaCl.

7. Mathematical Modeling

7.1 One-Site and Two-Site Multi-Constituent Models

For one-site and two-site multi-constituent models (MCB and TMC models), the relationship between the sand surface area covered by deposited IONP/rhamnolipid (A_P or A_R) and the deposited solid phase concentration (S_P and S_R) were calculated using conversion factors, which are:

$$\tau = \frac{A_P^{particle} * m_{sand}}{\rho_P * V_P^{particle}} \qquad (S7)$$

$$\zeta = \frac{N_A * A_R^{molecule} * m_{sand}}{M_w^R} \qquad (S8)$$

Where $A_P^{particle}$ is the area covered by a single iron oxide nanoparticle (m²/particle) and m_{sand} is the mass of the sand (g). ρ_P is the density of iron oxide(5.2 g cm⁻³) and $V_P^{particle}$ is a volume(m³) of the core iron oxide particle which has an diameter of 8nm. N_A is Avogadro's Number (6.02 x 10²³ molecules/mol), $A_R^{molecule}$ the area covered by a single rhamnolipid molecule and M_w^R represents the molecular weight of rhamnolipid(g mol⁻¹).

Using τ and ζ to convert S and S_{max} for IONP and rhamnolipid to their respective areas resulted:

$$\frac{A_P}{A_{total}} = \frac{\tau * S_P}{\tau * S_{max}^P} = \frac{S_P}{S_{max}^P} \qquad (S9)$$

$$\frac{A_R}{A_{total}} = \frac{\zeta * S_R}{\zeta * S_{max}^R} = \frac{S_R}{S_{max}^R} \quad (S10)$$

and A_{total} are all available surface area (single layer) for attachment/adsorption for both constituents, so:

$$A_{total} = \tau * S_{max}^P = \zeta * S_{max}^R \quad (S11)$$

Rearranging these equations yields:

$$S_{max}^R = \frac{\tau}{\zeta} * S_{max}^P \quad (S12)$$

To calculate τ and ζ, volumes of mono- and di- rhamnolipid were first estimated using Molinspiration (http://www.molinspiration.com/cgi-bin/properties) to be 625.35 Å^{-3} and 501.49 Å^{-3} , respectively. Assuming a spherical geometry both for mono- and di-rhamnolipid, the average area occupied by a single rhamnolipid molecule was then calculated as 1.033 nm^2 since the rhamnolipid used in this research is a mixture of 3:2 mono- and di-rhamnolipid.

Based on the hydrodynamic size of IONP, which is about 40 nm in DI water, the area occupied by an individual nanoparticle was calculated to be 1256.6 nm^2.

Then equation (S12) becomes:

$$S_{max}^R = 1.127 * S_{max}^P$$

which means the surface area for 1 µg g^{-1}(as iron) deposition of IONP can absorb 1.127 µg g^{-1} rhamnolipid. Complete monolayer coverage values of IONP and rhamnolipid biosurfactant were also estimated for 80-100 mesh Ottawa sand ($d_c = 0.165$mm), assuming spherical grains(Table S3); however, it should be noted that these values are conservative estimates, as sand surface topography heterogeneity will create substantially more available surface area than that estimated for a spherical geometry.

Table S3. Calculated rhamnolipid and IONP properties used when relating nanoparticle retention capacity to polymer adsorption capacity.

Property	Value	Units
Rhamnolipid area occupied	1.033	nm^2
Theoretical monolayer coverage for rhamnolipid ($d_c = 0.165$mm)	12.42	µg g^{-1}
Conversion factor	6.8847E3	m^2*g-sand g^{-1} rhamnolipid
IONP area occupied	1256.6	nm^2
Theoretical monolayer coverage for IONP ($d_c = 0.165$mm) as Fe	11.02	µg g^{-1}

7.2 Mathematical Model Comparisons and Selection

Four mathematical models (TSC, CFT, DDS and TRS models, Table S4) were explored to model experimental observations that had evidence of filter ripening (e.g. downward C/C0 plateau and hyper exponential retention profile). The fitted BTCs and retention profiles (RPs) are shown in Figure S9.

Table S4. Mathematical models used when filter ripening was suspected to have occurred. [12-14]

Models	Governing equations	Transport mechanism (other than advection and dispersion)	Fitted parameters*	Ref
Classical filtration theory model (CFT)	1. $\dfrac{\partial C}{\partial t} + \dfrac{\rho_b \partial S}{\theta_w \partial t} = D_h \dfrac{\partial^2 C}{\partial x^2} - v_p \dfrac{\partial S}{\partial x}$ 2. $\dfrac{\rho_b \partial S}{\theta_w \partial t} = k_{att} C$	Attachment (unlimited surface)	k_{att}	(12)
Depth dependent straining model (DDS)	1. $\dfrac{\partial C}{\partial t} + \dfrac{\rho_b \partial S}{\theta_w \partial t} = D_h \dfrac{\partial^2 C}{\partial x^2} - v_p \dfrac{\partial S}{\partial x}$ 2. $\dfrac{\rho_b \partial S}{\theta_w \partial t} = k_{att} C + k_{str} \Phi C$ 3. $\Phi = \dfrac{(d_c + x)^{-\beta}}{d_c}$	Attachment (unlimited surface), and Physical straining	k_{att}, k_{str}, β	(13), (14)

Two-site single-constituent model (TSC)	1.$\frac{\partial C}{\partial t} + \frac{\rho_b \partial S}{\theta_w \partial t} = D_h \frac{\partial^2 C}{\partial x^2} - v_p \frac{\partial S}{\partial x}$ 2.$\frac{\rho_b \partial S_1}{\theta_w \partial t} = k_{att} \Psi C$ 3.$\frac{\rho_b \partial S_2}{\theta_w \partial t} = k_{rip} \Phi C$ 4.$\Psi = 1 - \frac{S_1^p}{S_{1,max}^{\,p}} - \frac{S_1^R}{S_{1,max}^{\,R}} \ (0 \leq \Psi \leq 1)$ 5.$\Phi = \frac{S}{S_{1,max}} \ (\Phi \geq 0)$	Attachment (maximum capacity), filter ripening	$k_{att}, S_{max}, k_{rip}$	This study
Two-site ripening and straining model (TRS)	1.$\frac{\partial C}{\partial t} + \frac{\rho_b \partial S}{\theta_w \partial t} = D_h \frac{\partial^2 C}{\partial x^2} - v_p \frac{\partial S}{\partial x}$ 2.$\frac{\rho_b \partial S_1}{\theta_w \partial t} = k_{att} \Psi C$ 3.$\frac{\rho_b \partial S_2}{\theta_w \partial t} = k_{rip} \Phi C + k_{rip} \varphi C$ 4.$\Psi = 1 - \frac{S_1^p}{S_{1,max}^{\,p}} - \frac{S_1^R}{S_{1,max}^{\,R}} \ (0 \leq \Psi \leq 1)$ 5.$\Phi = \frac{S}{S_{1,max}} \ (\Phi \geq 0)$ 6.$\varphi = \frac{(d_c + x)^{-\beta}}{d_c}$	Attachment (maximum capacity), Filter ripening, Physical straining (Depth dependent)	$k_{att}, S_{max}, k_{str},$ β, k_{rip}	This study

nanoparticle attachment rate coefficient (k_{att}), nanoparticle physical straining rate coefficient (k_{str}), nanoparticle filter ripening rate coefficient (k_{rip}), physical straining empirical factor (β), S_{max} or $S_{1,max}$: maximum retention capacity (S_{max} or $S_{1,max}$).

As shown in Figure S9, the CFT and DDS models were not able to reproduce the downward plateau of the measured BTC, while the TSC and TRS model exhibited good performance in capturing both the characteristics of BTCs and RPs. However, the TRS model has 5 fitted parameters, and resulted in much larger 95% confidence intervals for same parameters than those fitted by the TSC model. Thus, the TSC model was selected for use in this study.
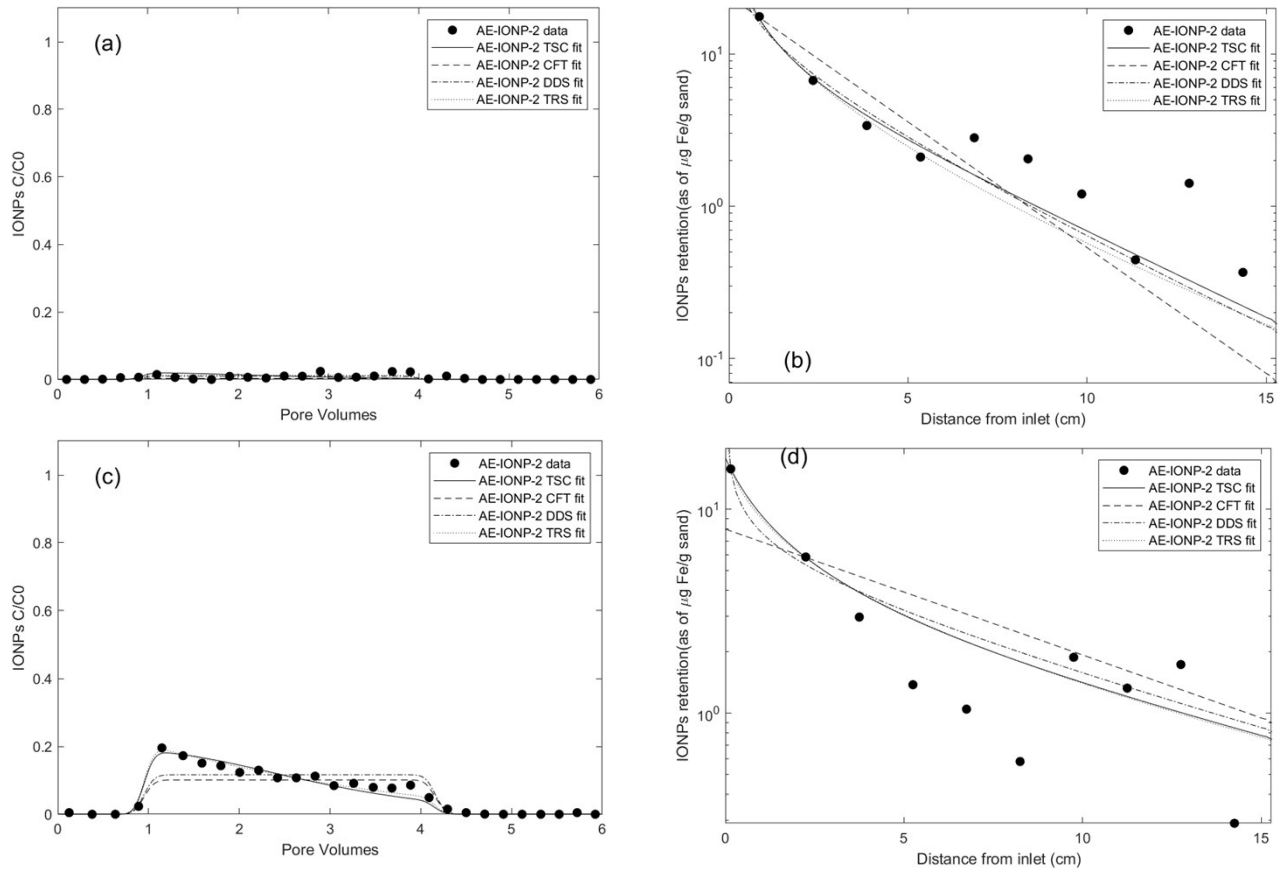
Figure S9: Experimental and fitted effluent breakthrough curves and retention profiles using MFT and TSC models for IONP only column (a-b) and 50 mg L^{-1} rhamnolipid preflood column (c-d).

For IONP transport with rhamnolipid in aerobic medium columns, four mathematical models (MFT, TSC, MCB and TMC models, Table S5) were examined and the best fit model was selected. The fitted BTCs and RPs obtained using these models are shown in Figure S10.

Table S5 Mathematical models considered when IONPs transport with rhamnolipid in aerobic medium columns. [15, 16]

Models	Governing equations	Transport mechanism (other than advection and dispersion)	Fitted parameters*	Ref

Modified filtration theory model (MFT)	1. $\dfrac{\partial C}{\partial t} + \dfrac{\rho_b \partial S}{\theta_w \partial t} = D_h \dfrac{\partial^2 C}{\partial x^2} - v_p \dfrac{\partial S}{\partial x}$ 2. $\dfrac{\rho_b \partial S}{\theta_w \partial t} = k_{att}\Psi C$ 3. $\Psi = \dfrac{S_{max} - S}{S_{max}}$	Attachment (maximum or limiting capacity of Porous media)	k_{att}, S_{max}	(15)
Two-site single-constituent model (TSC)	1. $\dfrac{\partial C}{\partial t} + \dfrac{\rho_b \partial S}{\theta_w \partial t} = D_h \dfrac{\partial^2 C}{\partial x^2} - v_p \dfrac{\partial S}{\partial x}$ 2. $\dfrac{\rho_b \partial S_1}{\theta_w \partial t} = k_{att}\Psi C$ 3. $\dfrac{\rho_b}{\theta_w}\dfrac{\partial S_2}{\partial t} = k_{rip}\Phi C$ 4. $\Psi = 1 - \dfrac{S_1^p}{S_{1,max}^p} - \dfrac{S_1^R}{S_{1,max}^R}\ (0 \le \Psi \le 1)$ 5. $\Phi = \dfrac{S}{S_{1,max}}\ (\Phi \ge 0)$	Attachment (maximum capacity), filter ripening	$k_{att}, S_{max}, k_{rip}$	This study
One-site multi-constituent model (MCB)	1. $\dfrac{\partial C^i}{\partial t} + \dfrac{\rho_b \partial S^i}{\theta_w \partial t} = D_h \dfrac{\partial^2 C^i}{\partial x^2} - v_p \dfrac{\partial C^i}{\partial x}$ 2. $\dfrac{\rho_b \partial S^i}{\theta_w \partial t} = k_a^i \Psi C^i - k_d^i \dfrac{\rho_b}{\theta_w} S^i$ 3. $\Psi = 1 - \dfrac{S_1^p}{S_{1,max}^p} - \dfrac{S_1^R}{S_{1,max}^R}(0 \le \Psi \le 1)$	Attachment (maximum capacity), Competitive adsorption of additives	$k_a\ (k_{att}, k_{ads}), S_{max}$	(16)
Two-site multi-constituent model (TMC)	See mathematical modelling part in this study	Attachment (maximum capacity), filter ripening Competitive adsorption of additives	$k_a\ (k_{att}, k_{ads}), S_{max}, k_{rip}$	This study

* nanoparticle attachment rate coefficient (k_{att}), nanoparticle physical straining rate coefficient (k_{str}), nanoparticle filter ripening rate coefficient (k_{rip}), Rhamnolipid adsorption rate coefficient (k_{ads}), physical straining empirical factor (β), S_{max} or $S_{1,max}$: maximum retention capacity (S_{max} or $S_{1,max}$).

As shown in Figure S10, the TMC model exhibited the best fits to the experimental data for AE-R10 as it accounts for rhamnolipid adsorption and IONP ripening attachment. Thus, the TMC model was selected for application to IONP transport with 10mg L^{-1} rhamnolipid in aerobic medium (IS = 50.4mM). For IONP

transport with 50 mg L^{-1}, since the introduction of ripening rate did not improve the fitting(figure 10 c and
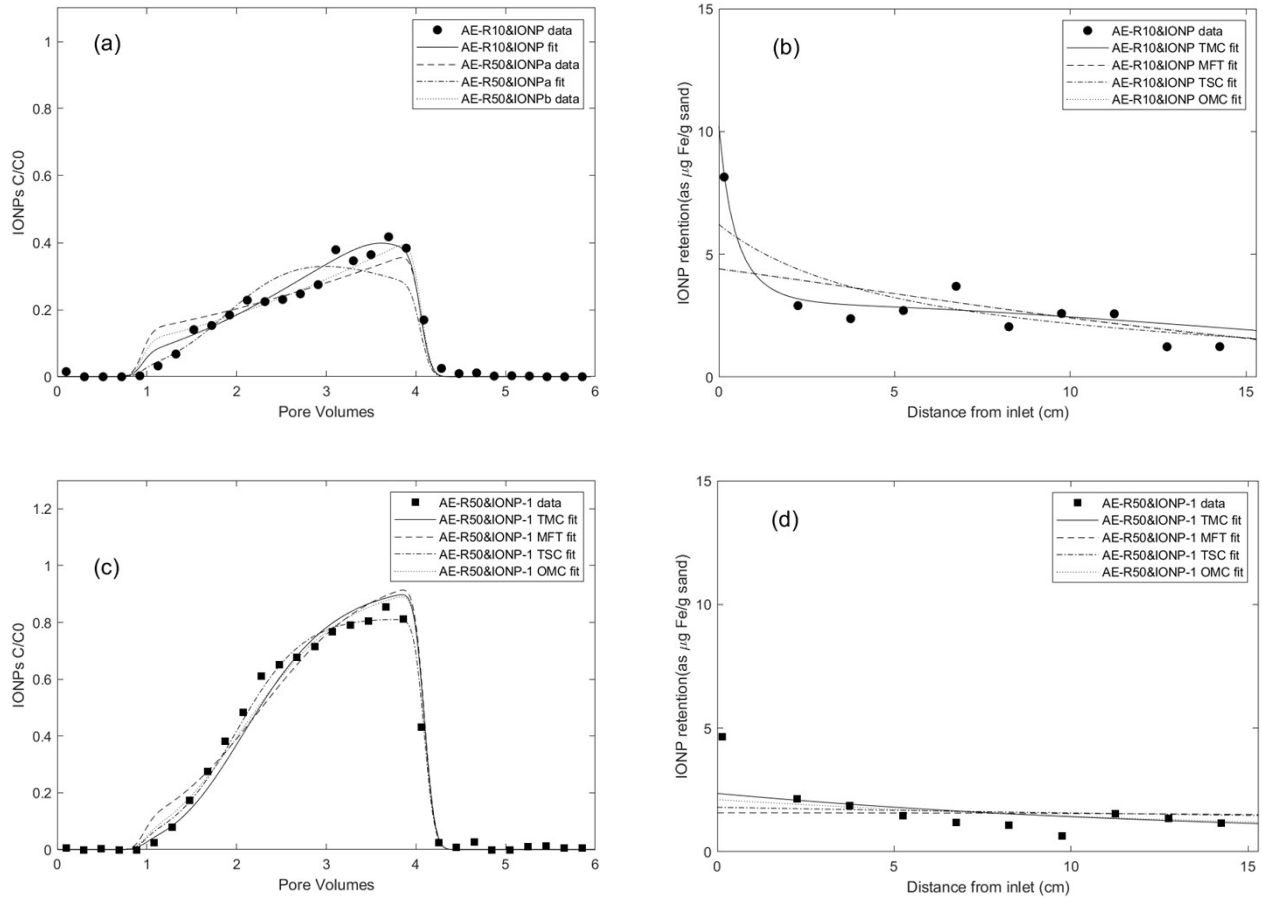

Figure S10. Experimental and fitted effluent breakthrough curves and retention profiles using TSM, MFT, TSC andMCB models for columns co-injected with and 10 (a-b) and 50 mg L^{-1} (c-d) rhamnolipid.

d) significantly, MCB model was employed to reduce the fitting parameters (ripening rate).

The MFT and MCB models were chosen for IONP transport experiments when using 10mM NaCl as background electrolyte since there was no indication of occurrence of a filter ripening process and the competitive adsorption of rhamnolipid was evident based on the observed increase in solid-phase IONP concentration with distance from the inlet. Figure 5 in the paper demonstrated that both models can accurately describe nanoparticle transport and retention behaviors.

Mathematical models employed for different column experiments in this research were summarized in Table S6.

Table S6. Mathematical models used to simulate IONO and rhamnolipid transport.

Column identifier	Model	Transport Mechanisms Accounted
AE-IONP-1, AE-IONP-2, AE-R10_IONP, AE-R50_IONP	TSC	Attachment, filter ripening
AE-R10&IONP, AE-R10_R10&IONP	TMC	Attachment, filter ripening, rhamnolipid adsorption
NaCl-IONP-1, NaCl-IONP-2	MFT	Attachment
AE-R50_R50&IONP-1, AE-R50&IONP-1, AE-R50&IONP-2, AE-R50_R50&IONP-2, NaCl-R50&IONP-1, NaCl-R50&IONP-2, NaCl-R50_R50&IONP	MCB	Attachment, rhamnolipid adsorption

7.3 Weighting Factors

In this study, two weighting factors (β and γ) in the objective function were selected for each experiment that resulted in a best fit, based on visual examination and evaluation of R^2 and 95% confidence interval of parameters. β and γ are in a range of 0 to 1 with a constrain that $\beta + \gamma = 1$.

Table S7. Weighting factors used to fit BTCs and RPs obtained from the column experiments.

| Column identifier	β (BTC weighting factor)	γ (RP weighting factor)
AE-IONP-1, AE-IONP-2,	0.1	0.9
AE-R10_IONP, NaCl-IONP-1, NaCl-IONP-2	0.2	0.8
AE-R50_IONP, AE-R10&IONP	0.4	0.6
AE-R50&IONP-2, NaCl-R50_R50&IONP	0.7	0.3
AE-R50&IONP-1, AE-R10_R10&IONP	0.8	0.2
NaCl-R50&IONP-1, NaCl-R50&IONP-2	0.9	0.3
AE-R50_R50&IONP-1, AE-R50_R50&IONP-2	1	0

8. Explanation of relatively large 95% confidence intervals for four column experiments (AE-R50&IONPa, AE-R50&IONPb, AE-R50_R50&IONPa, AE-R50_R50&IONPb.).

Using AE-R50&IONPa as an example, assuming a nanoparticle attachment rate constant (1e^{-4} s^{-1}), the optimization function presented in the paper (sum of the squared residuals) was calculated over a range of S_{max} and k_{ads} values. The corresponding contour plots are shown in Figure S11. Here, from the top view (Figure S11(a)) and side views of the optimization function contour (Figure S11(b) and (c)), it is evident that the fitted values of S_{max}(6 µg/g) and k_{ads}(2.5e^{-5} s^{-1}) correspond to the global minimum, validating the optimization function used for model fitting. This contour plot also suggests that the optimization function is relatively insensitive to both the S_{max} and k_{ads} parameters, since the calculated squared residuals remain close to the objective function minimum from the start(0) to the end of the domain tested, leading to relatively large 95% confidence intervals of S_{max} and k_{ads}. Similar results were observed for the other three column experiments.

(a)
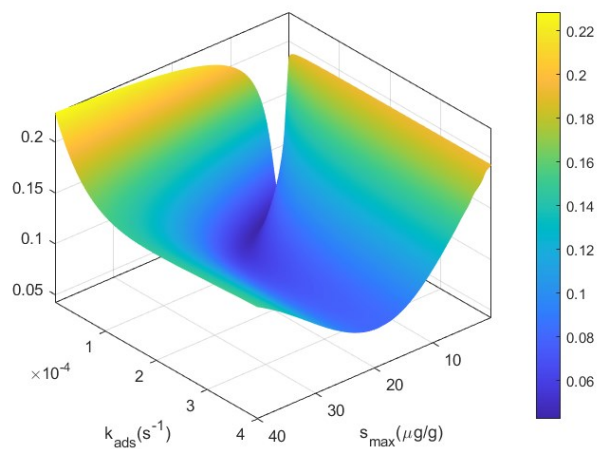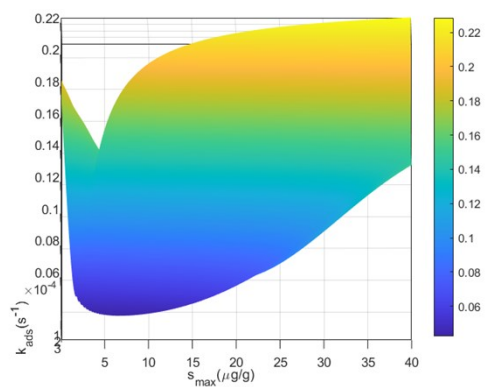
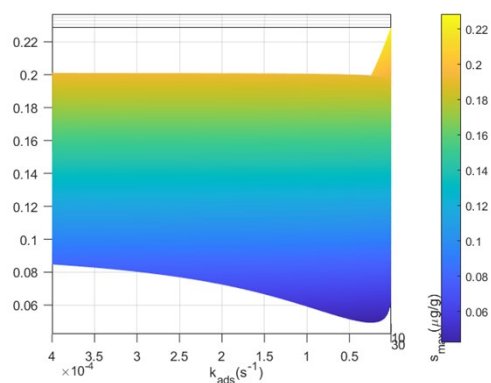(b)   (c)

Figure S11. Contour plot of the common logarithm of the values of the optimization function with variable S_{max} and k_{ads} for AE-R50&IONPa column. (a) Top view, (b) side view from S_{max}, (c) side view from k_{ads}.

References

1. B. Deraguin and L. Landau, Theory of the stability of strongly charged lyophobic sols and of the adhesion of strongly charged particles in solution of electrolytes, *Acta Physicochim: USSR*, 1941, **14**, 633-662.
2. E. J. W. Verwey, Theory of the stability of lyophobic colloids, *The Journal of Physical Chemistry*, 1947, **51**, 631-636.
3. T. Phenrat, N. Saleh, K. Sirk, H.-J. Kim, R. D. Tilton and G. V. Lowry, Stabilization of aqueous nanoscale zerovalent iron dispersions by anionic polyelectrolytes: adsorbed anionic polyelectrolyte layer properties and their effect on aggregation and sedimentation, *Journal of Nanoparticle Research*, 2007, **10**, 795-814.
4. A. R. Petosa, D. P. Jaisi, I. R. Quevedo, M. Elimelech and N. Tufenkji, Aggregation and deposition of engineered nanomaterials in aquatic environments: role of physicochemical interactions, *Environ Sci Technol*, 2010, **44**, 6532-6549.
5. B. Faure, G. Salazar-Alvarez and L. Bergstrom, Hamaker constants of iron oxide nanoparticles, *Langmuir*, 2011, **27**, 8659-8664.
6. G. Fritz, V. Schädler, N. Willenbacher and N. J. Wagner, Electrosteric stabilization of colloidal dispersions, *Langmuir*, 2002, **18**, 6381-6390.
7. J. Xu, S. Sun, Z. Wang, S. Peng, S. Hu and L. Zhang, pH-Induced evolution of surface patterns in micelles assembled from dirhamnolipids: dissipative particle dynamics simulation, *Phys Chem Chem Phys*, 2018, **20**, 9460-9470.
8. S. Bhattacharjee and M. Elimelech, Surface element integration: A novel technique for evaluation of DLVO interaction between a particle and a flat plate, *Journal of Colloid and Interface Science*, 1997, **193**, 273-285.
9. K. A. Guzman, M. P. Finnegan and J. F. Banfield, Influence of surface potential on aggregation and transport of titania nanoparticles, *Environ Sci Technol*, 2006, **40**, 7688-7693.
10. Y. Wang, H. Zhu, M. D. Becker, J. Englehart, L. M. Abriola, V. L. Colvin and K. D. Pennell, Effect of surface coating composition on quantum dot mobility in porous media, *Journal of Nanoparticle Research*, 2013, **15**.
11. W. Li, D. Liu, J. Wu, C. Kim and J. D. Fortner, Aqueous aggregation and surface deposition processes of engineered superparamagnetic iron oxide nanoparticles for environmental applications, *Environ Sci Technol*, 2014, **48**, 11892-11900.
12. K.-M. Yao, M. T. Habibian and C. R. O'Melia, Water and waste water filtration. Concepts and applications, *Environmental science & technology*, 1971, **5**, 1105-1112.
13. S. A. Bradford, J. Simunek, M. Bettahar, M. T. Van Genuchten and S. R. Yates, Modeling colloid attachment, straining, and exclusion in saturated porous media, *Environ Sci Technol*, 2003, **37**, 2242-2250.
14. Y. Wang, J. H. Kim, J. B. Baek, G. W. Miller and K. D. Pennell, Transport behavior of functionalized multi-wall carbon nanotubes in water-saturated quartz sand as a function of tube length, *Water Res*, 2012, **46**, 4521-4531.
15. Y. Li, Y. Wang, K. D. Pennell and L. M. Abriola, Investigation of the transport and deposition of fullerene (C60) nanoparticles in quartz sands under varying flow conditions, *Environ Sci Technol*, 2008, **42**, 7174-7180.
16. M. D. Becker, Y. Wang, K. D. Pennell and L. M. Abriola, A multi-constituent site blocking model for nanoparticle and stabilizing agent transport in porous media, *Environmental Science: Nano*, 2015, **2**, 155-166.